Geophysical Research Letters

Supporting Information for

Rupture Along 400 km of the Bering Fracture Zone in the Komandorsky Islands Earthquake (M_W 7.8) of 17 July 2017

Thorne Lay[1], Lingling Ye[2], Yefei Bai[3], Kwok Fai Cheung[3], Hiroo Kanamori[2], Jeffrey Freymueller[4], Grigory M. Steblov[5,6], and Mikhail G. Kogan[7]

[1]Department of Earth and Planetary Sciences, University of California Santa Cruz, Santa Cruz, California, USA, [2]Seismological Laboratory, California Institute of Technology, Pasadena, California, USA, [3]Department of Ocean and Resources Engineering, University of Hawaii at Manoa, Honolulu, Hawaii, USA, [4]Geophysical Institute, University of Alaska Fairbanks, Fairbanks, Alaska, USA, [5]Schmidt Institute of Physics of the Earth RAS, Moscow, Russia, [6]Geophysical Survey RAS, Obninsk, Kaluga Region, Russia, [7]Lamont-Doherty Earth Observatory, Columbia University, New York, USA.

Correspondence to: Thorne Lay, tlay@ucsc.edu

Contents of this file

Additional Supporting information (Files uploaded separately).

Movie A1. Animation of the back-projections from North America and Europe.

Introduction

Data processing and rupture parameterization details are provided in Text S1, with Figures S1 to S14 providing supporting information about the seismicity, back-projection imaging, and finite-fault modeling.

Text S1

We estimated GPS displacements in the ITRF2008 reference frame from two separate solutions. There were no significant differences for the two overlapping stations, AC60 and PETS, so solutions were selected from one or the other.

The Geophysical Survey of the Russian Academy of Sciences data center is used to process the data of the Kamchatka GPS Network including BRNG (Bering Island) and PETS (Petropavlovsk). We use the GAMIT/GLOBK software in three steps (Herring et al. 2010): (1) 24-hour data spans of our stations are combined with 8 nearest sites of the International GNSS Service; (2) Regional daily solutions of step 1 are treated as quasi-observations and combined with global daily solutions available from Scripps Orbit and Permanent Array Center (SOPAC) or from MIT using a Kalman filter; (3) Combined daily solutions of step 2 are constrained with the reference frame ITRF2008 updated at MIT and transformed relative to the North American plate. This last transformation has little impact on the displacements because of the short time span considered (less than 3 weeks total). Static offsets are estimated from mean station positions for 9 days before and 9 days after the earthquake.

The University of Alaska Fairbanks processed the data from the remaining sites, all part of the Plate Boundary Observatory (PBO). We use the GIPSY software and the analysis procedures described in Fu & Freymueller (2012). Each individual station was processed in Precise Point Positioning (PPP) mode (Zumberge et al., 1997) using the JPL final orbits and clock products. Positions from all stations for a single day from a large area encompassing all of Alaska and including PETS (but not BRNG) are combined into a single daily loosely-constrained solution, which is then transformed into the ITRF2008 reference frame. Static offsets are estimated from mean station positions for 4 days before and 4 days after the earthquake.

For the kinematic rupture model, we assume continuous rupture from the onset, parameterizing relatively long-duration subfault ruptures to allow the rupture to expand or not during the initial interval of weak radiation. For the unilateral rupture model we use 21 subfaults along strike with 12 km lengths and 8 subfaults along dip with 4 km widths. The hypocenter is 12.5 km below sea level at 54.443°N, 168.857°E. The rupture expansion velocity is 2.15 km/s. The subfault source durations are parameterized with 10 2-s rise-time triangles, offset by 2-s each, permitting up to 22 s long subfault durations. For the bilateral rupture model we use 38 subfaults along strike with 12 km lengths and 8 subfaults along dip with 4 km widths. The hypocenter is 12.5 km below sea level at 54.593°N, 168.957°E. The rupture expansion velocity is 3.0 km/s. The subfault source durations are parameterized with 8 2-s rise-time triangles, offset by 2-s each, permitting up to 22 s long subfault durations.

Additional References

Fu, Y., & Freymueller, J. T. (2012). Seasonal and long-term vertical deformation in the Nepal Himalaya constrained by GPS and GRACE measurements. *J. Geophys. Res*., *117*, B03407, doi:10.1029/2011JB008925.

Zumberge, J. F., Heflin, M. B., Jefferson, D. C., Watkins, M. M., & Webb, F. H. (1997). Precise point positioning for the efficient and robust analysis of GPS data from large networks. *J. Geophys. Res., 102*(B3), 5005–5017, doi:10.1029/96JB03860.

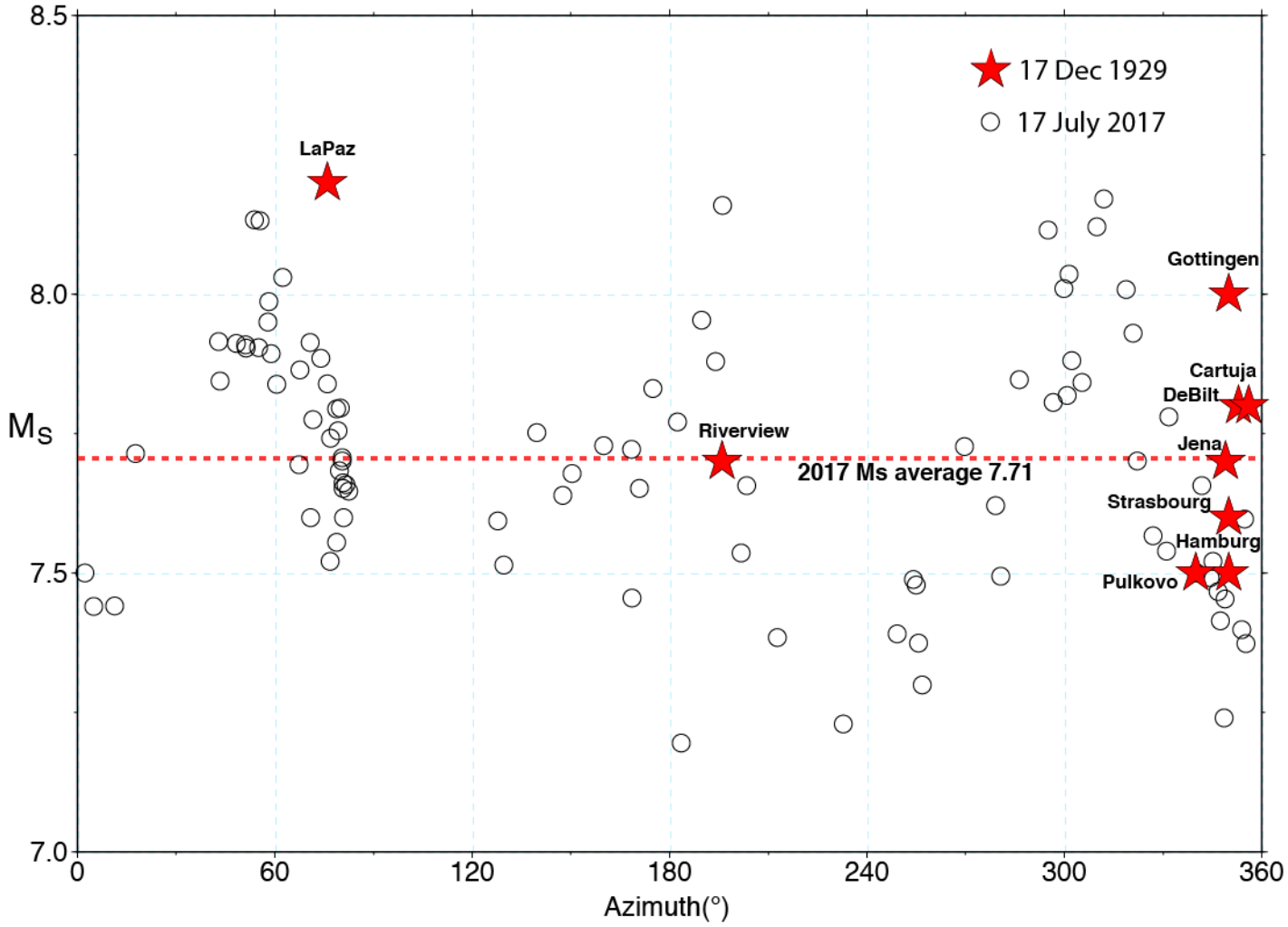

Figure S1. Measurements of M_S at stations with different azimuths for the 17 December 1929 Near Islands earthquake (red stars) and the 17 July 2017 Komandorsky Islands earthquake (open circles). Amplitude data for the 1929 event are from Gutenberg's notepad, and M_S values for the 2017 event are from the USGS/NEIC. Similar M_S at different azimuths suggests that two events are of comparable size.

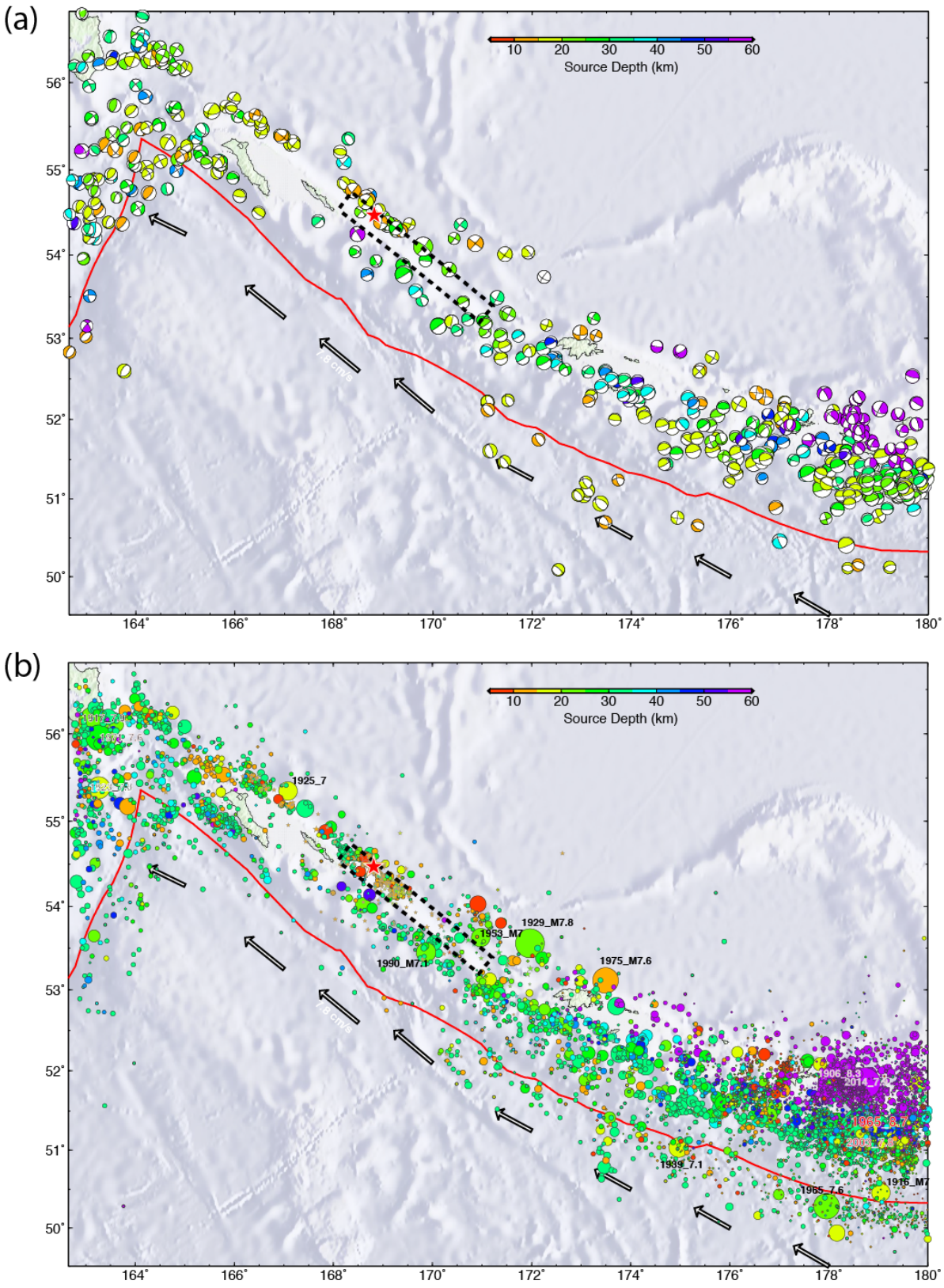

Figure S2. (a) Moment tensor solutions from the GCMT for the western Aleutians, color-coded by depth. (b) USGS-NEIC seismicity for the western Aleutians from 1900 to 2017, color-coded by depth.

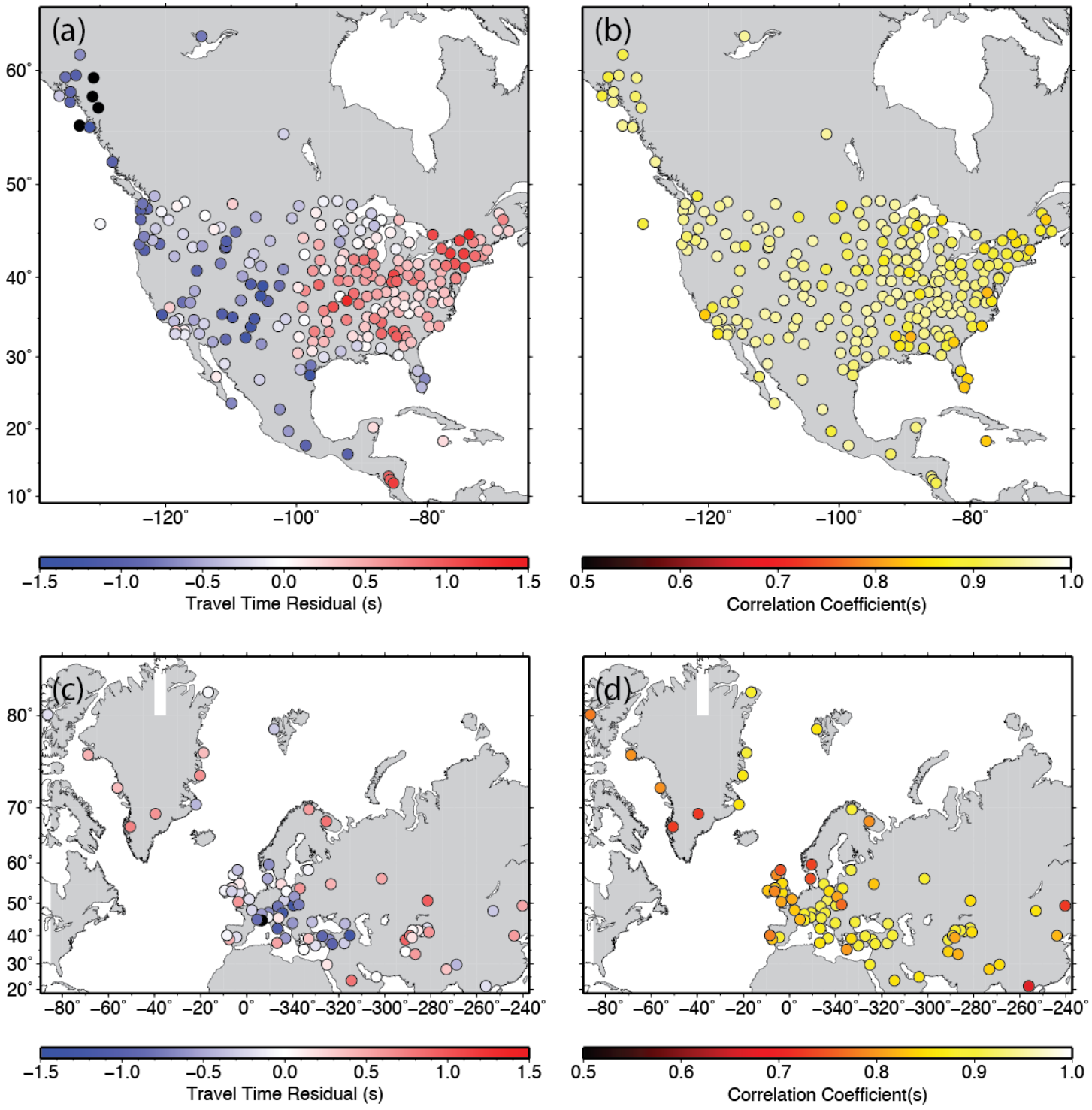

Figure S3. Station locations for large aperture arrays of broadband seismic stations for which filtered short-period *P* waves signals are used in back-projections for the 17 July 2017 earthquake rupture. (a) and (b) show the North American stations used with the time shifts from multi-station broadband correlations (a) and the correlation coefficients (b). (c) and (d) show the Eurasian and Greenland stations used with the time shifts from multi-station broadband correlations (c) and the correlation coefficients (d).

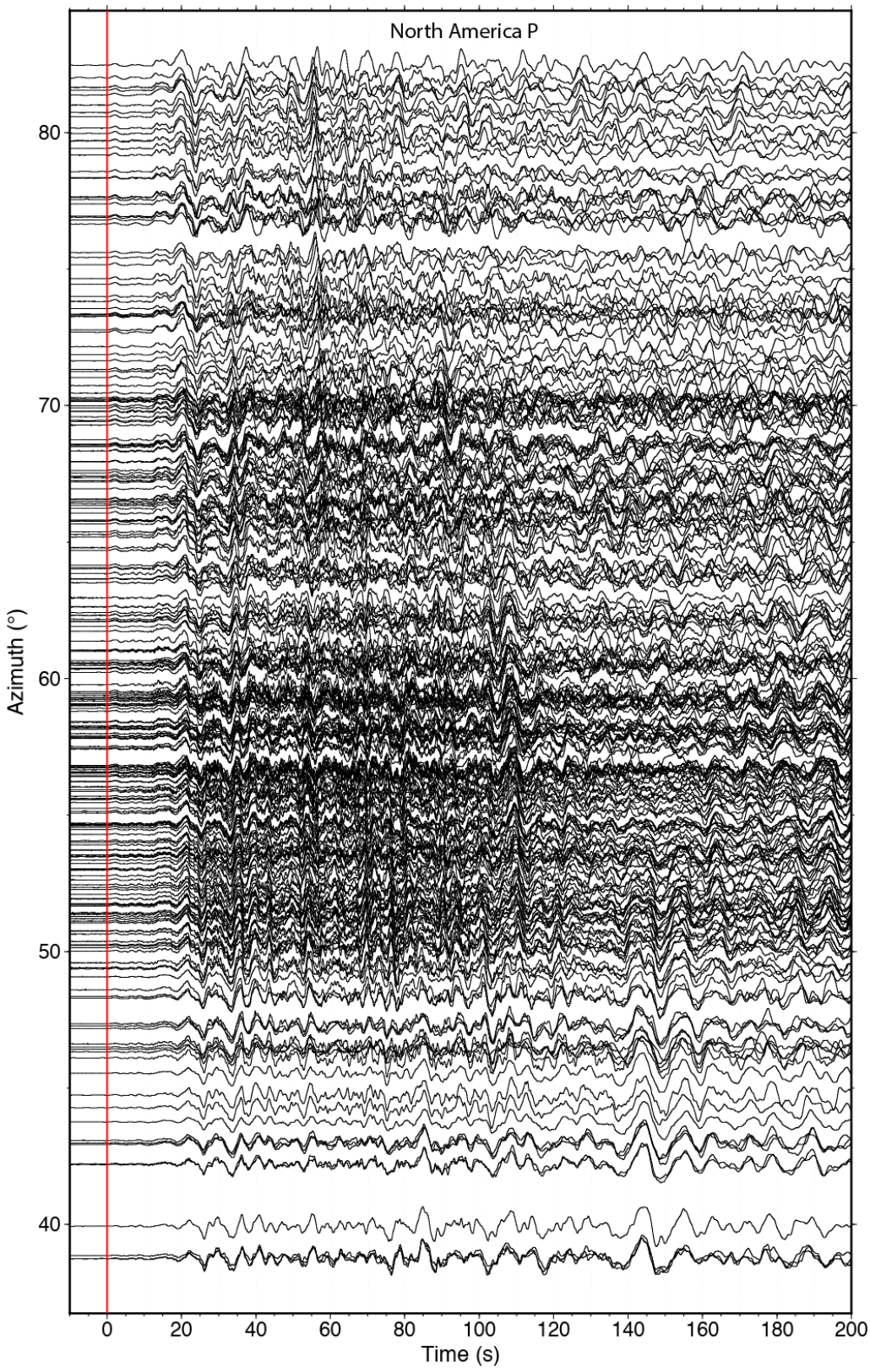

Figure S4. Azimuthal plot of the broadband *P* waves from North American stations in Figure S3a with time corrections applied. Note the ~15 s delay before strong arrivals.

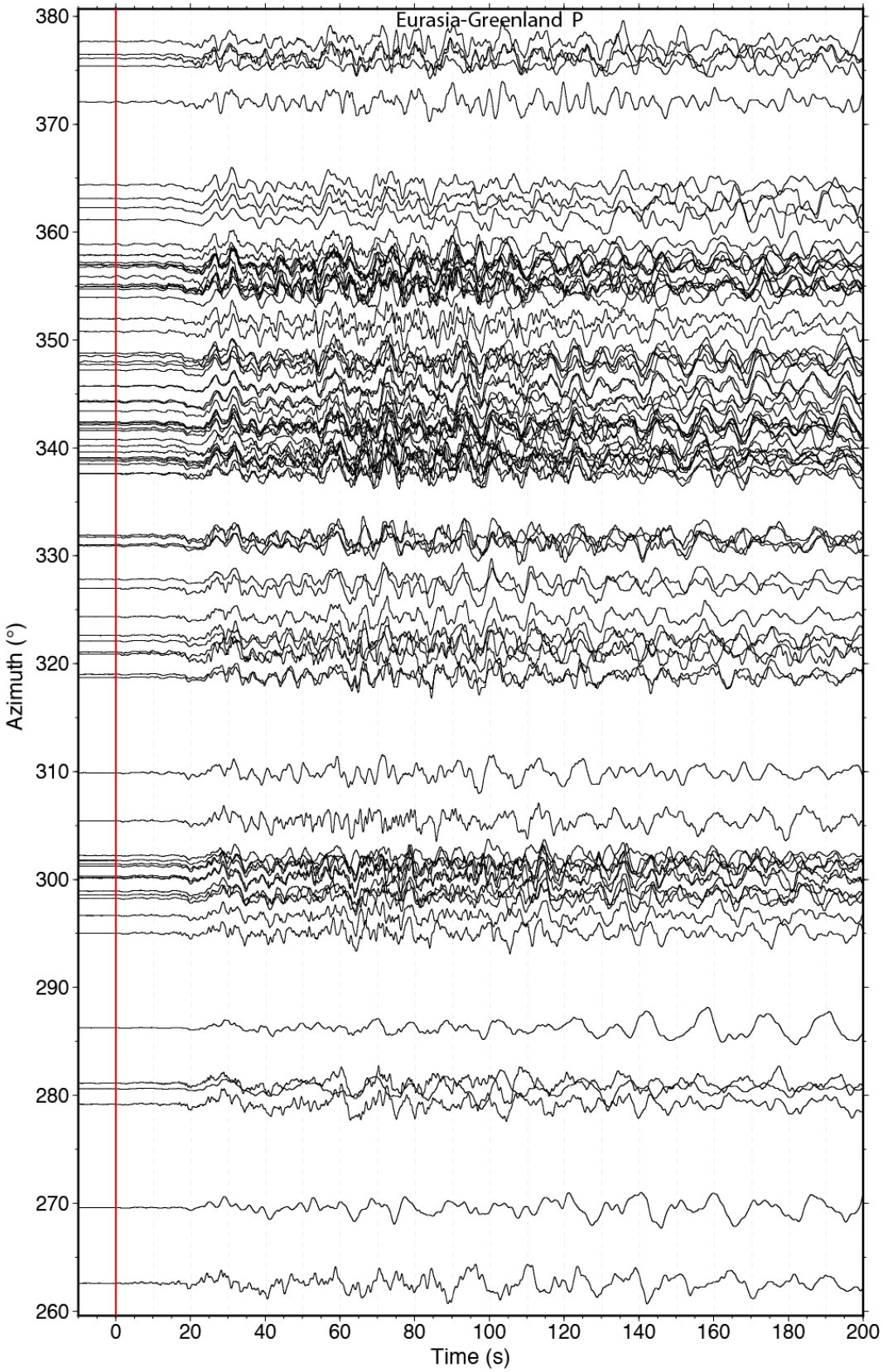

Figure S5. Azimuthal plot of the broadband *P* waves from Eurasian and Greenland stations in Figure S3c with time corrections applied. Note the ~15 s delay before strong arrivals.

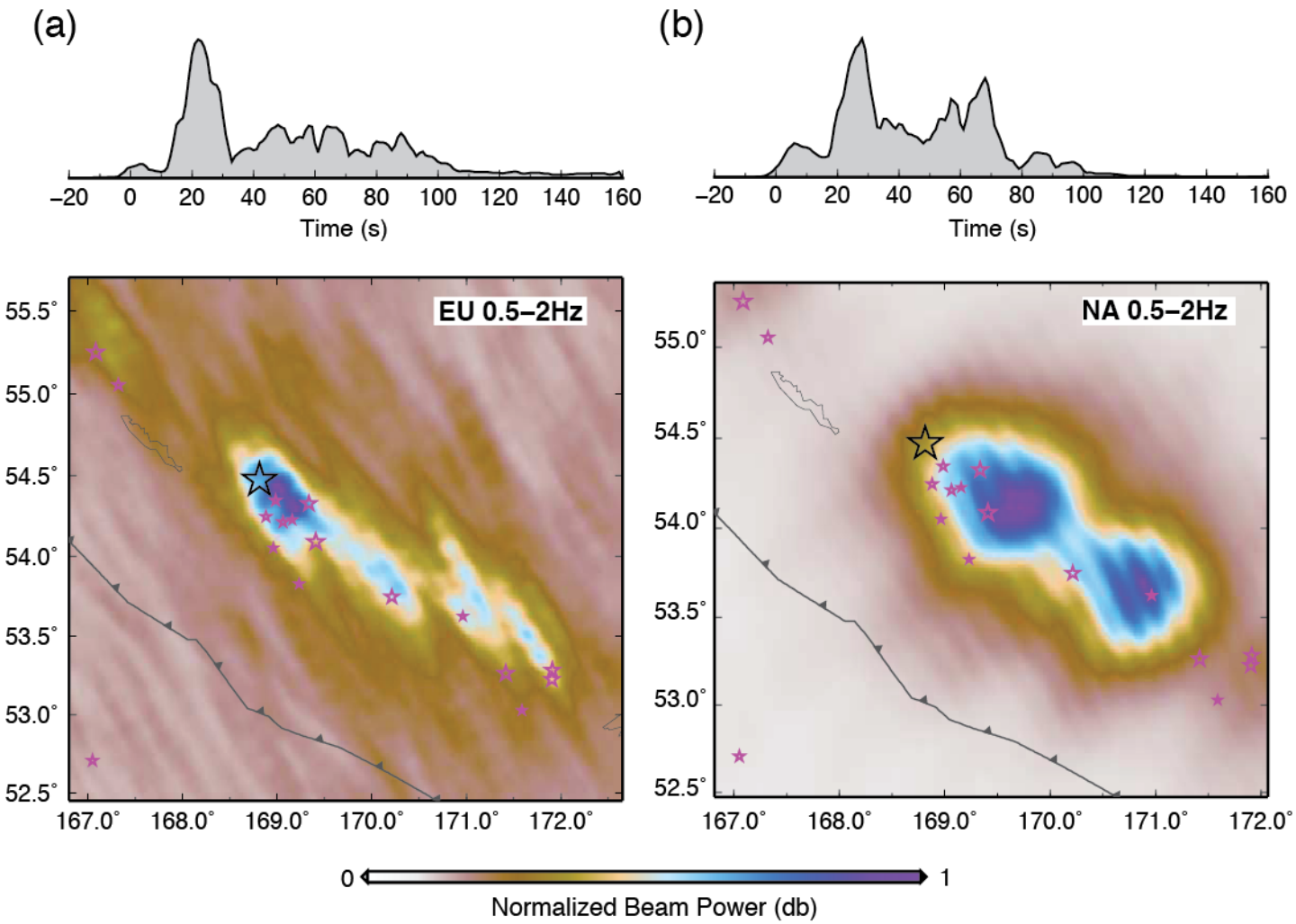

Figure S6. Time-integrated stacks of back-projection beam power for 0.5-2.0 Hz *P* waves for the signals from Eurasia and Greenland (a) and from North America (b). The fourth-root stacked beam power as a function of time for the two geometries is shown above each map. The black stars indicate the USGS/NEIC epicenter and the magenta stars are large aftershocks in the first day.

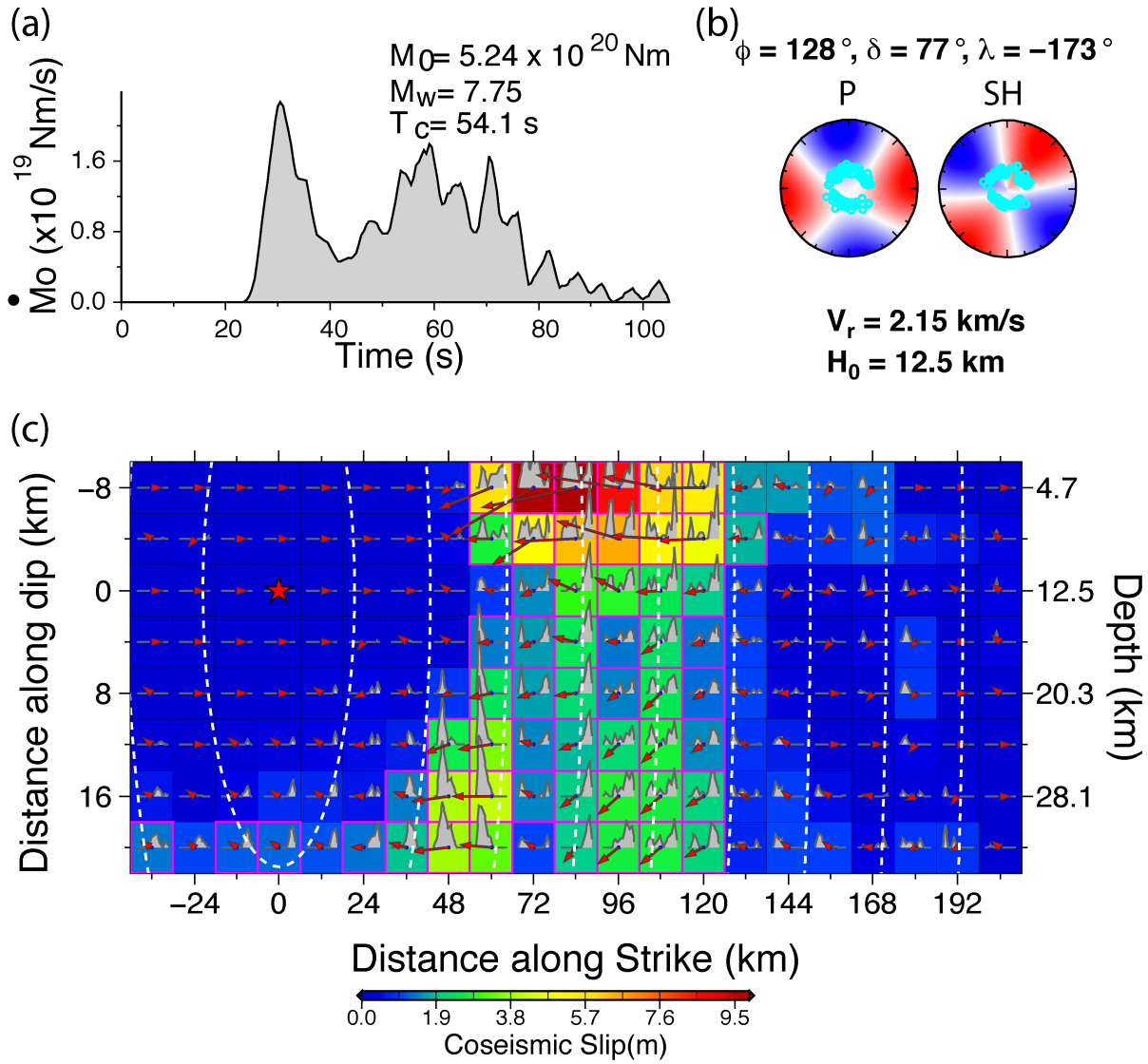

Figure S7. Unilateral finite-fault slip model for the 17 July 2017 Komandorsky Islands earthquake from inversion of teleseismic *P* and *SH* ground displacement waveforms. The moment rate function is shown in (a), with the seismic moment, M_0, M_W and centroid time, T_c being indicated. The average faulting geometry is shown in (b), along with the data distribution and radiation patterns for *P* and *SH* signals in lower hemisphere equal area projections. Red quadrants are compressional motions for *P* waves and clockwise rotation for *SH* waves. The rupture expansion velocity, V_r and hypocenter depth H_0 are shown. The slip distribution on the fault is shown in (c), as viewed from the southwest. Vectors indicate average slip and rake of the hanging wall (Komandorsky Sliver) relative to the footwall (Bering Plate). The color palette indicates the slip magnitude for each subfault. The subfault moment rate functions are shown by the polygons inside each slip, with total durations of up to 22 s. Isochrones of rupture front location in 10 s intervals are indicated by white dashes. The hypocenter is indicated by the red star.

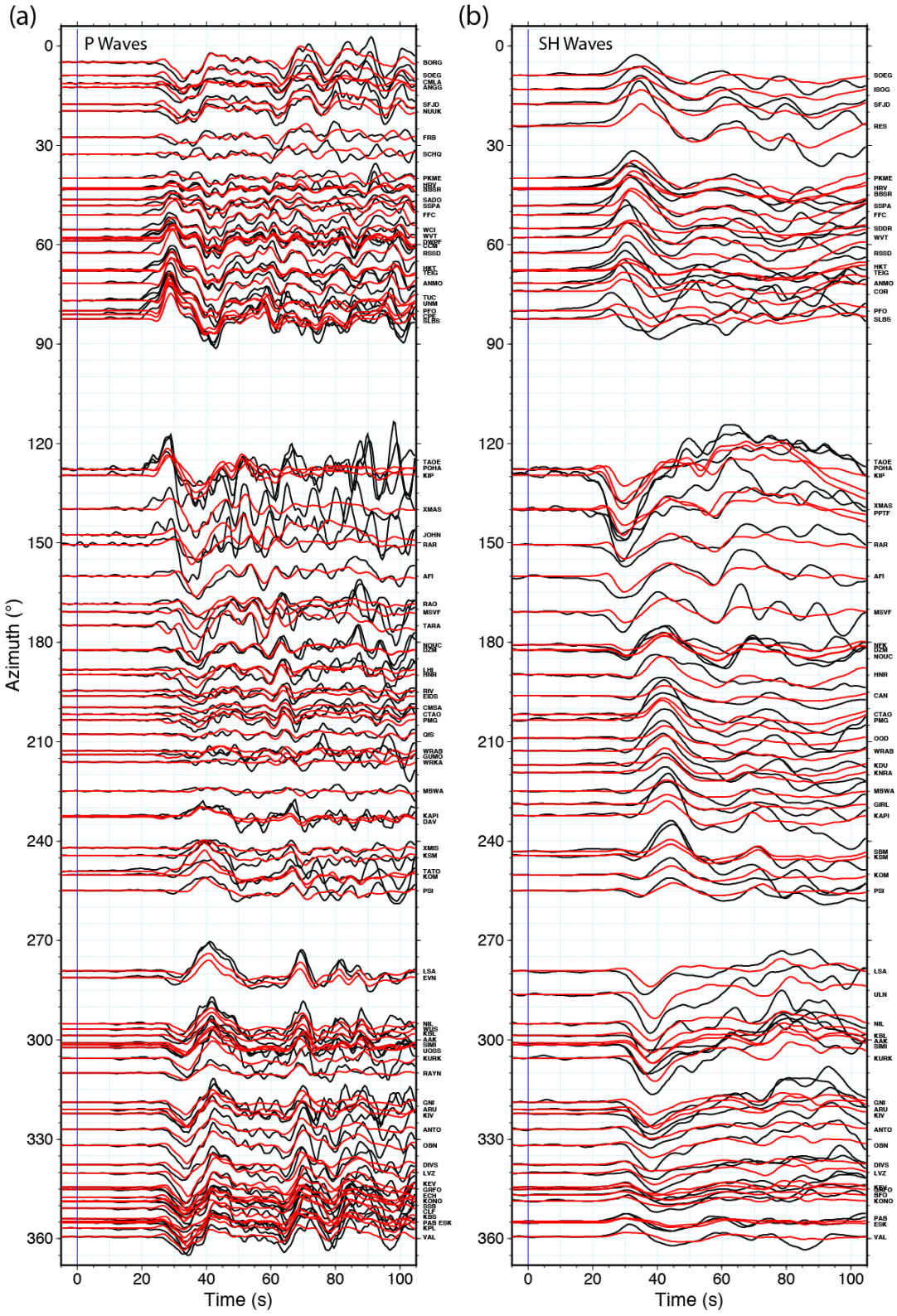

Figure S8. Azimuthal distributions of (a) *P* wave observations (black curves) and synthetics (red curves) for the unilateral fault model in Figure S7, and (b) *SH* wave observations (black curves) and synthetics (red curves).

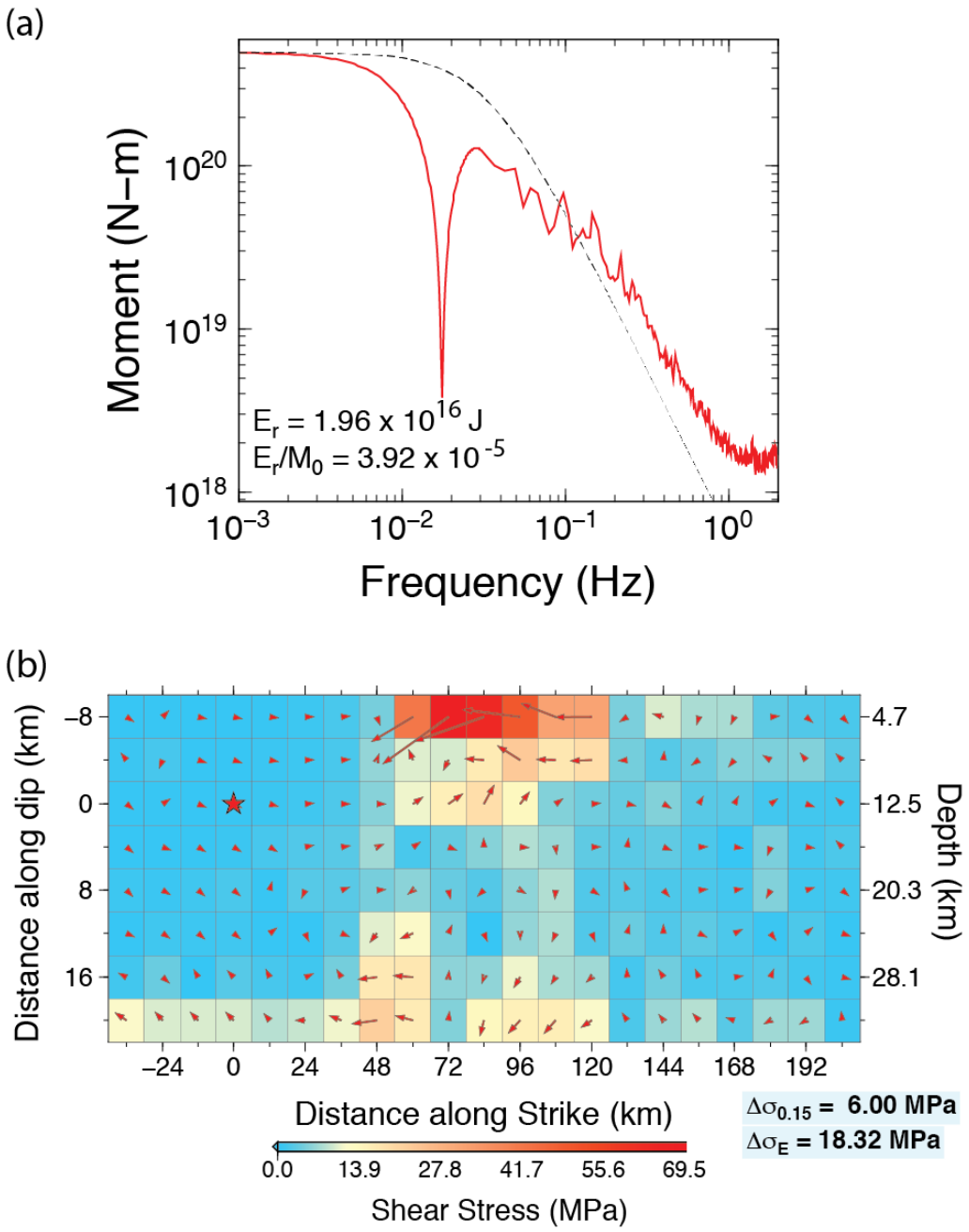

Figure S9. (a) Far-field source spectrum for the unilateral model (Figure S7) obtained by combining the spectrum of the moment rate function for frequencies less than 0.05 Hz with the logarithmic average of globally distributed *P* wave spectra for frequencies higher than 0.05 Hz. The dotted line is a reference ω-squared spectrum with corresponding seismic moment and a stress factor of 3 MPa. The broadband radiated seismic energy, E_r, estimated from the teleseismic *P* wave observations using the method of Ye et al. (2016), and the seismic moment-scaled value are shown. (b) Static shear stress for the unilateral slip model for the 17 July 2017 Komandorsky Islands earthquake with the magnitude and direction for each subfault being shown. The average static shear stress drop for the model is 6 MPa using a procedure that removes all subfaults with seismic moment less than 15% of the peak subfault seismic moment. The slip-weighted average stress drop obtained using the method of Ye et al. (2016) gives a higher value of 18 MPa.

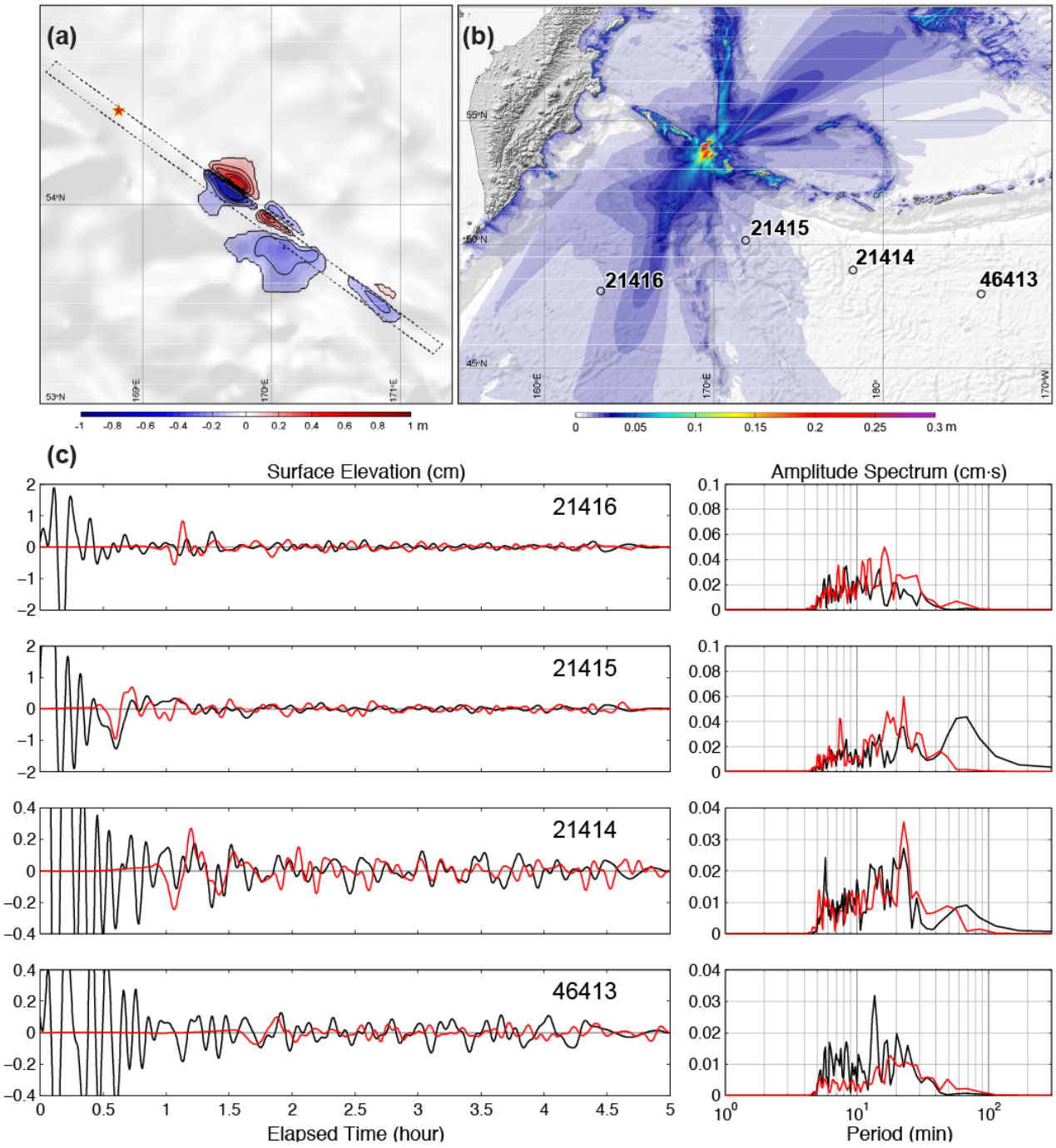

Figure S10. Predicted tsunami from the unilateral faulting model. (a) Final seafloor deformation with the red star indicating the epicenter and the dash line delineating projection of the faulting model on the seafloor. (b) Predicted tsunami amplitude and DART stations (circles) considered in this study. (c) Comparison of filtered sea surface recordings (black traces) at DART stations with predictions (red). The recorded and predicted time series were filtered to remove signals shorter than 5 min period and the full 5-hr time series were used in the computation of the amplitude spectra. The strike-slip faulting and position of the stations results in weak tsunami waves, but the timing and height of long-period arrivals provide bounds on the source.

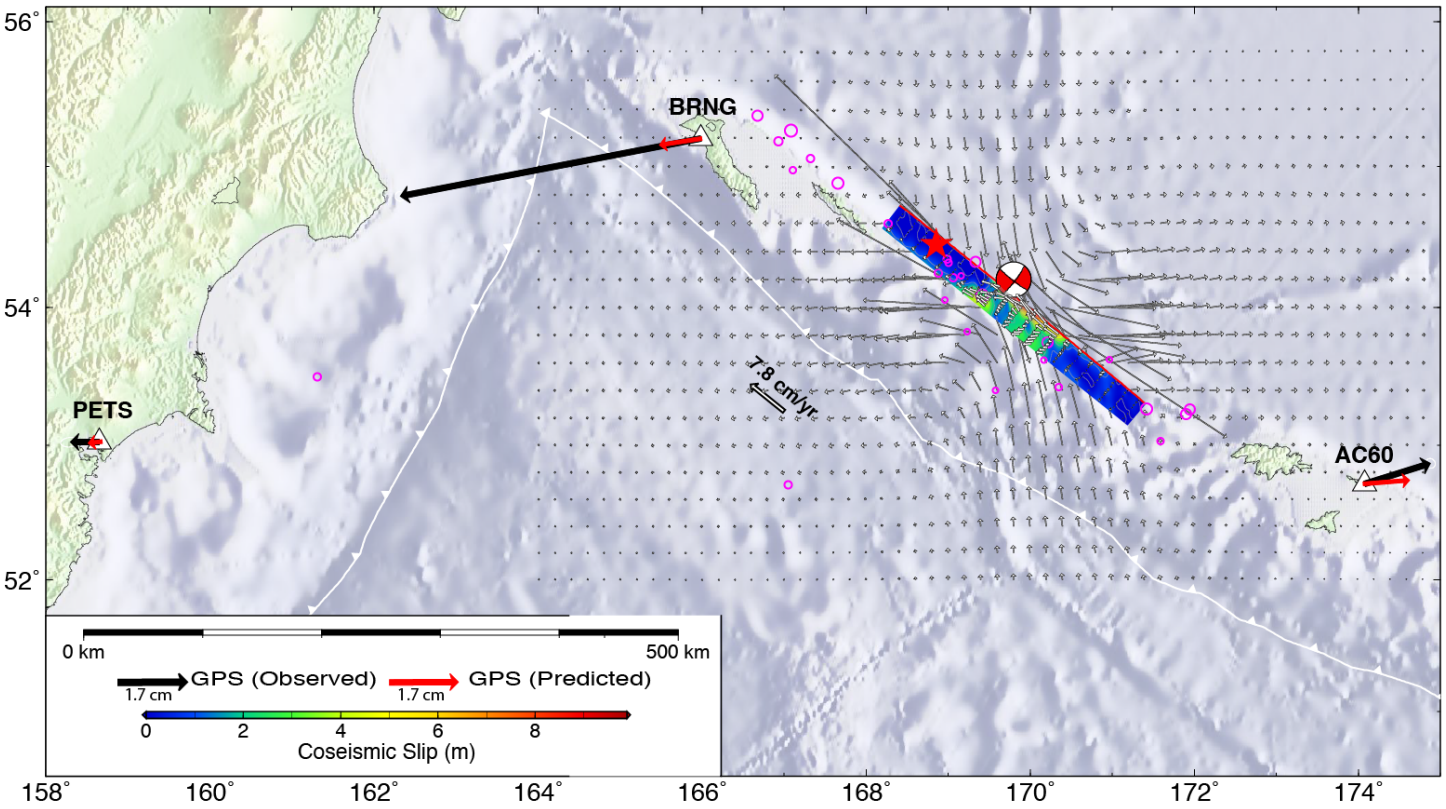

Figure S11. Prediction of GPS horizontal motions at stations BRNG (Bering Island), AC60 and PETS for the unilateral slip model. The observed GPS deformations are black arrows, the predicted values at those locations are red arrows. The grid of vectors indicates the spatial variation of predicted horizontal surface motions on 1/20th scale. The unilateral slip model location is shown in the rectangle, with early aftershock locations indicated by magenta circles and the *W*-phase moment tensor solution shown by the red focal mechanism.

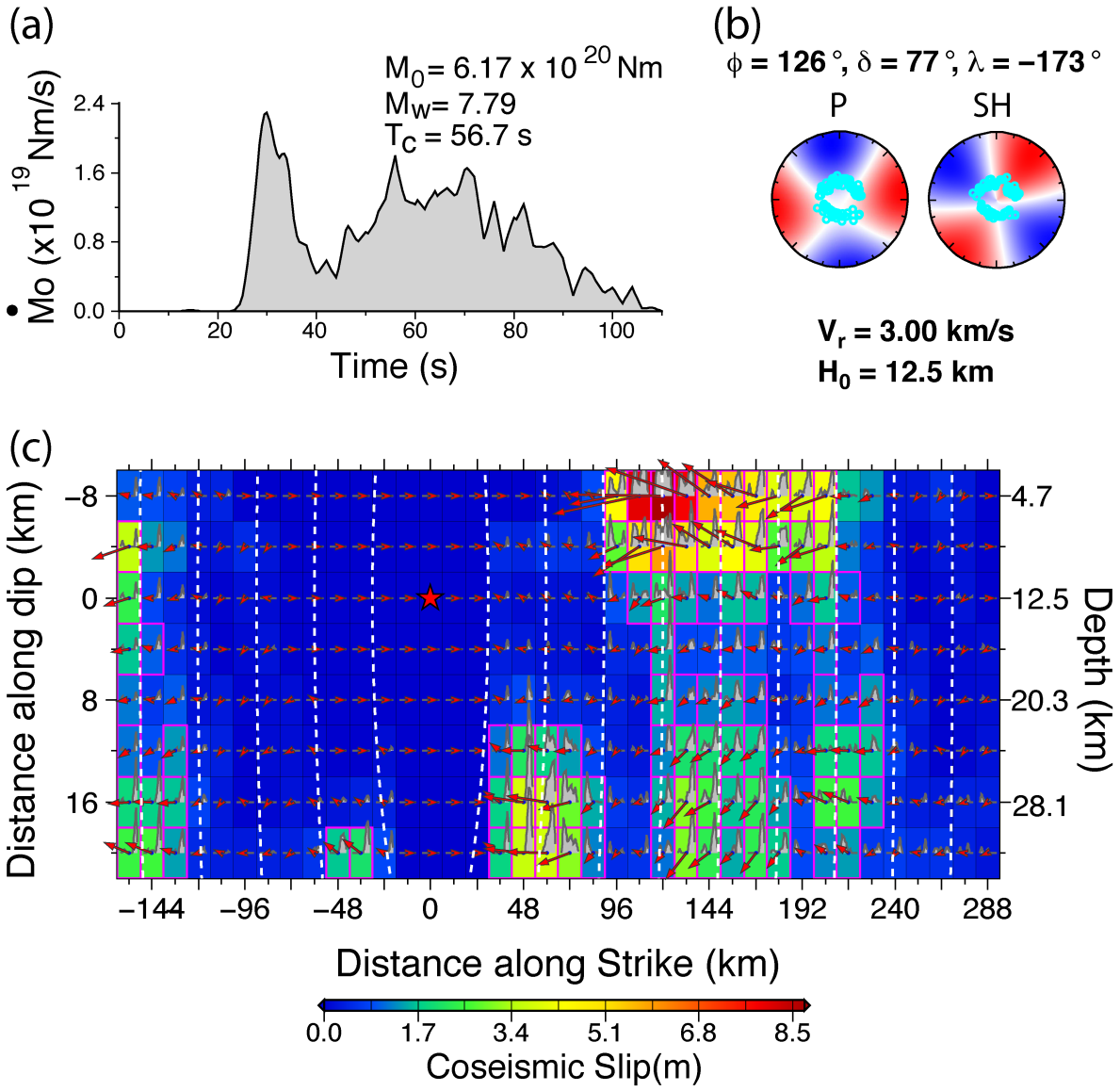

Figure S12. Preferred bilateral finite-fault slip model for the 17 July 2017 Komandorsky Islands earthquake from inversion of teleseismic *P* and *SH* waveforms. The moment rate function is shown in (a), with the seismic moment, M_0, M_W and centroid time, T_c being indicated. The average faulting geometry is given in (b), along with the data distribution and radiation patterns for *P* and *SH* signals in lower hemisphere equal area projections. Red quadrants are compressional motions for *P* waves and clockwise rotation for *SH* waves. The rupture expansion velocity, V_r and hypocenter depth H_0 are shown. The slip distribution on the fault is shown in (c), as viewed from the southwest. Vectors indicate average slip and rake of the hanging wall (Komandorsky Sliver) relative to the footwall (Bering Plate). The color palette indicates the slip magnitude for each subfault. The subfault moment rate functions are shown by the polygons inside each slip, with total durations of up to 18 s. Isochrones of rupture front location in 10 s intervals are indicated by white dashes. The hypocenter is indicated by the red star. The model is shown in map view in Figures 2 and 4.

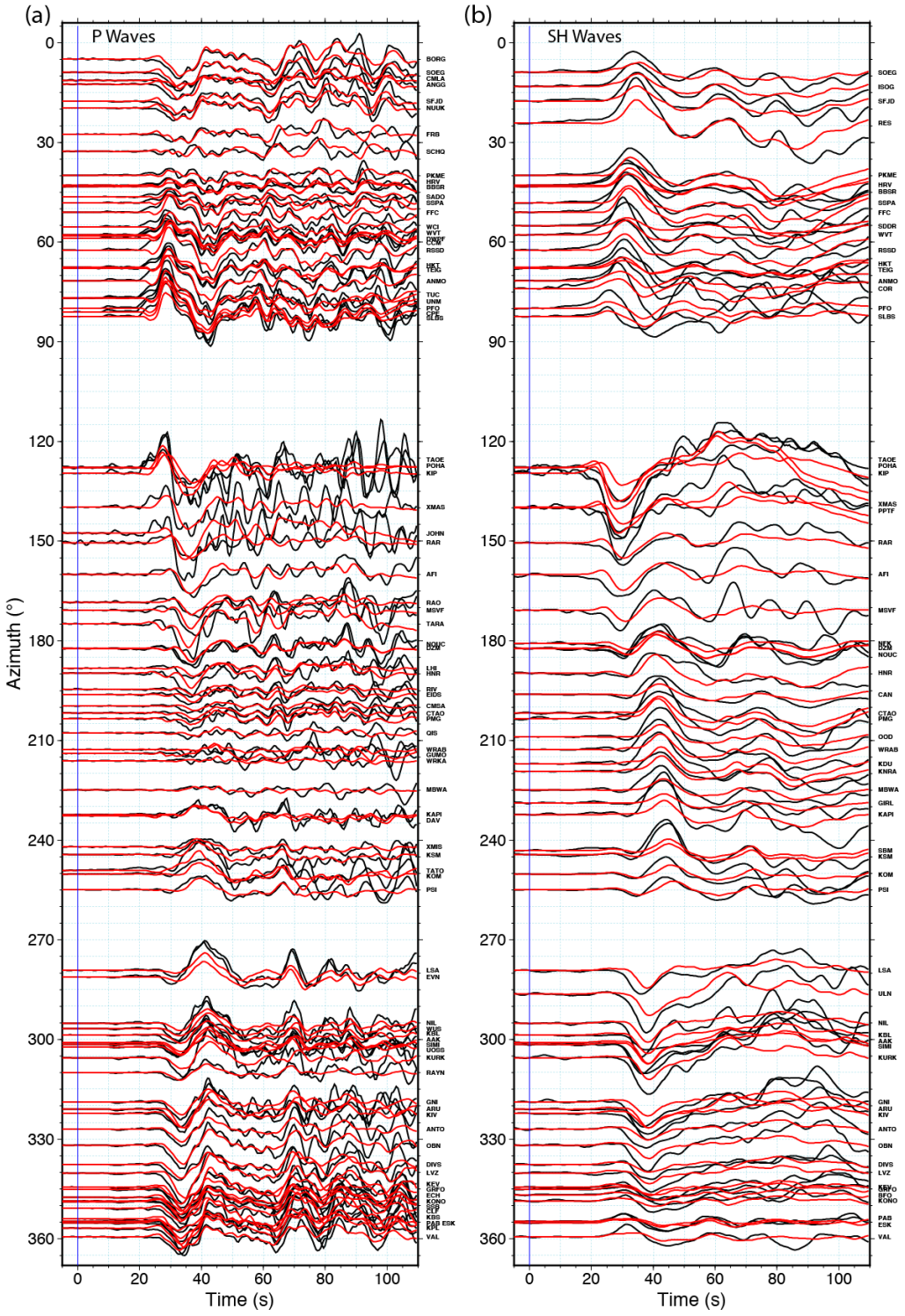

Figure S13. Azimuthal distributions of (a) *P* wave observations (black curves) and synthetics (red curves) for the preferred bilateral fault model (Figures 2, 4, S12), and (b) *SH* wave observations (black curves) and synthetics (red curves).

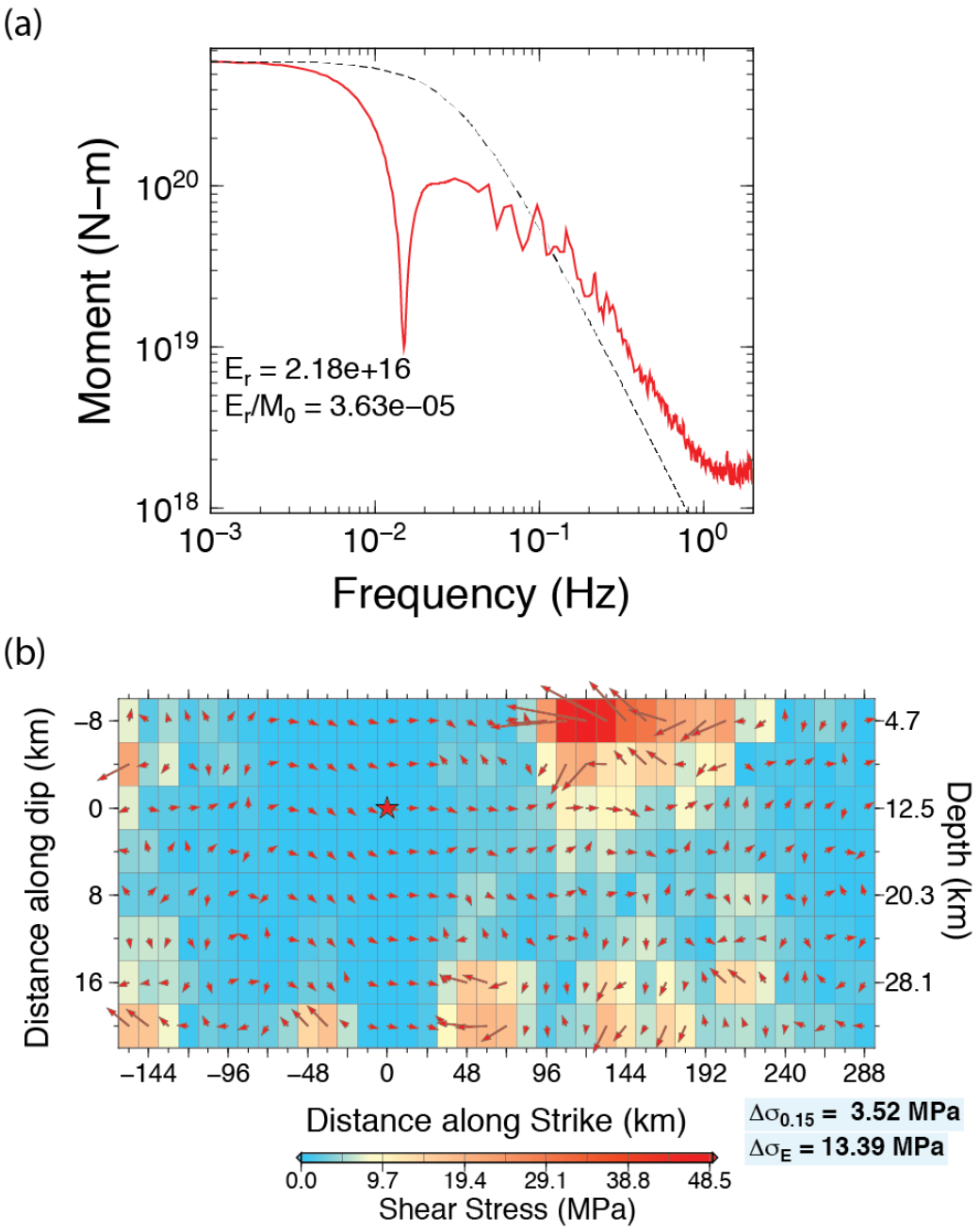

Figure S14. (a) Far-field source spectrum for the preferred bilateral model (Figures 2, 4, S12) obtained by combining the spectrum of the moment rate function for frequencies less than 0.05 Hz with the logarithmic average of globally distributed *P* wave spectra for frequencies higher than 0.05 Hz. The dotted line is a reference ω-squared spectrum with corresponding seismic moment and a stress factor of 3 MPa. The broadband radiated seismic energy, E_r, estimated from the teleseismic *P* wave observations using the method of Ye et al. (2016), and the seismic moment-scaled value are shown. (b) Static shear stress for the unilateral slip model for the 17 July 2017 Komandorsky Islands earthquake with the magnitude and direction for each subfault being shown. The average static shear stress drop for the model is 3.5 MPa using a procedure that removes all subfaults with seismic moment less than 15% of the peak subfault seismic moment. The slip-weighted average stress drop obtained using the method of Ye et al. (2016) gives a higher value of 13.4 MPa.

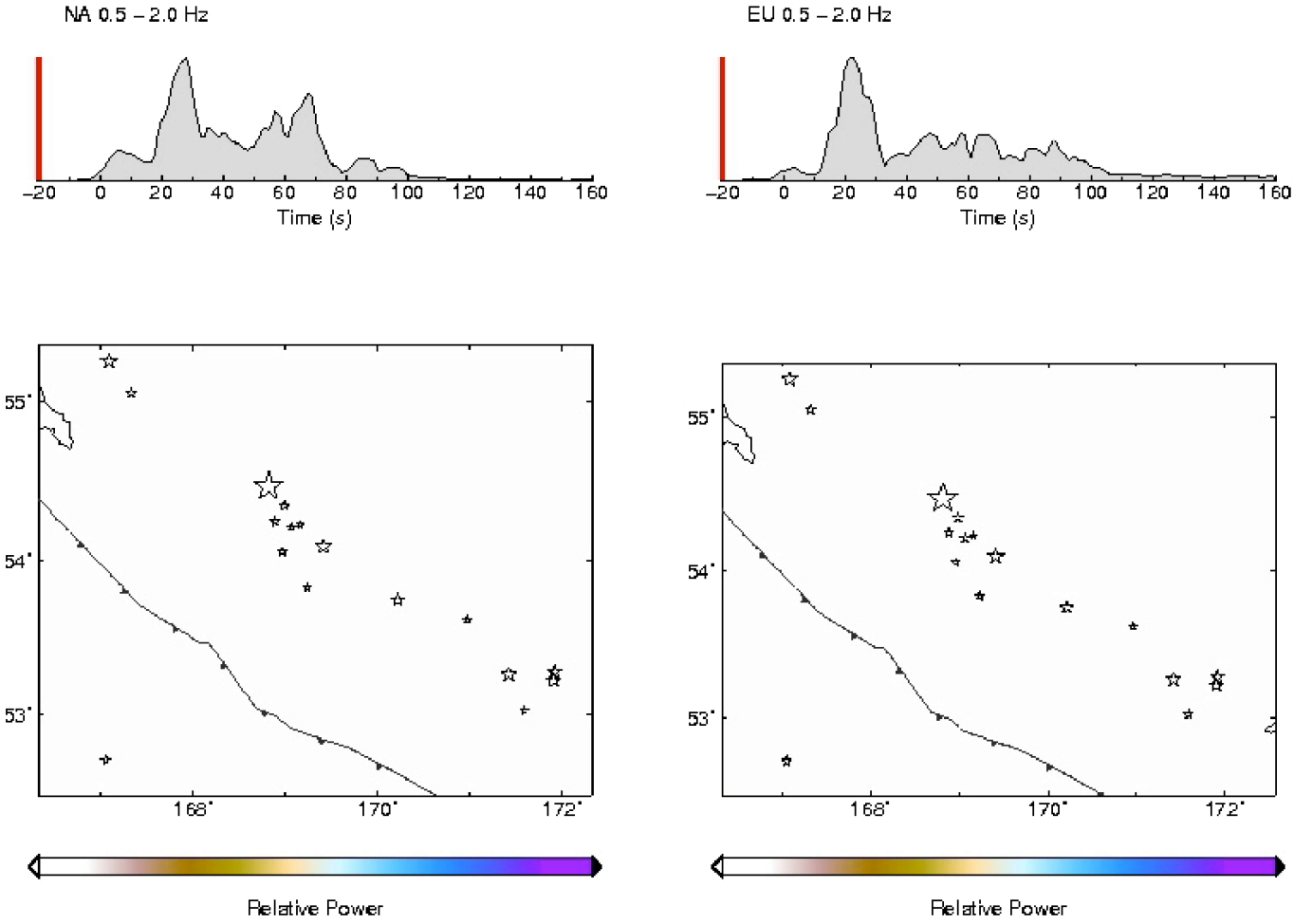

Animation A1. Back-projection of 0.5-2.0 Hz *P* wave data from the large aperture networks in North America (left) and Eurasia-Greenland (right) (see Figure S3). The fourth-root beam power is shown around the source region. The large star is the 17 July 2017 mainshock epicenter. Smaller stars are aftershocks in the first day.